Arch. Metall. Mater. **70** (2025), 1, 351-357

DOI: https://doi.org/10.24425/amm.2025.152552

S. PAULSINGARAYAR[1*], S.J.D.V. KUMAR[2], S. MARICHAMY[3], K. ANANDAVELU[3]

MACHINING BEHAVIORS AND SURFACE INVESTIGATION ON UDIMET L-605 ALLOY

This article is primarily concerned with the turning of Udimet L-605 alloy, which is crucial for a variety of applications, including the production of parts for the automotive, marine, and aircraft sectors. According to the researchers' recommendation, dry machining was preferable for this machining, and the studies were conducted using a PVD-coated TiAlN-TiN tungsten carbide cutting tool insert. Depth of cut during the machining process is essential for enhancing surface smoothness and reducing tool wear during the turning process. Increased cutting zone temperature brought on by deeper cutting causes increased tool wear and subpar surface finish. In this study, a greater emphasis was placed on the surface morphology for the machined surface's better and worse surface finishes. The peak and valley profiles created on the machined surface are mostly determined by kurtosis and skewness. The AFM study offered a clear indication of it. The average roughness of 34.77 nm was attained. Nearly 23% tool tip interface temperature was increased with increase of depth of cut.

Keywords: Udimet alloy; Machining; Surface morphology; Tool temperature; AFM

1. Introduction

The super alloy Udimet has a great frictional resistance and is based on nickel. It is made using the powder metallurgy technique. It is created as a material for turbine discs found in nuclear reactors that cool themselves with radioactive gas as well as other aircraft components that operate with elevated temperatures. The Udimet-L 605 has received numerous approvals from the airline industry. It was mainly used in the turbine blades, muffles, and combustion chamber. According to area-weight measurements, the Udimet-L605 alloy has the best impact resistance. Udimet-L605 has been shown to perform more effectively than the best titanium alloy, IMI 550, and to be stronger to other alloys, especially at extreme velocities. As a titanium alternative, the Udimet-L605 may be ideal for fan containment equipment in supersonic aircraft [1,2]. Surface excellence, which is crucial for the aerospace and nuclear industries, is very hard to acquire [3-4]. Thermo-electric machining is accomplished using wire electric discharge. On the factory floor, the WEDM process is widely used for the fabrication of dies, the creation of prototypes, and the intricately shaped manufacturing of tough components in the aviation and automobile sectors [5]. One of the key factors in the formation of chips is the extreme temperatures created during chip removal. Super alloys, on the other hand, maintain their distinctive mechanical capabilities at elevated temperatures due to their poor thermal conductivity. The machinability of super alloys is severely hampered by this circumstance. When chipping off super alloys, more force is needed. High temperatures develop in the cutting zone as a result of this force. Because of the material's poor heat conductivity, the cutting tool absorbs this high temperature. As is common knowledge, the cutting tool's wear is accelerated by the high temperatures in the cutting area. As a result, machining super alloys is a major challenge. To remove chips from materials with challenging machinability, researchers have experimented with a variety of techniques. Cryogenic treatment [6,7], cryogenic machining [8-10] and minimum quantity lubrication machining process [11-14] attracted more attention in the manufacturing field.

2. Materials and methods

The turning method in this investigation used commercially available Udimet L-65 alloy with a diameter of 50 mm and a length of 100 mm. The table below is a summary of the alloy's chemical composition. This study preferred dry machining, as

[1] DEPARTMENT OF MECHANICAL ENGINEERING, NPR COLLEGE OF ENGINEERING AND TECHNOLOGY, NATHAM, TAMILNADU
[2] DEPARTMENT OF MECHANICAL ENGINEERING, SSM INSTITUTE OF ENGINEERING AND TECHNOLOGY, DINDIGUL, TAMILNADU
[3] DEPARTMENT OF MECHANICAL ENGINEERING, MRK INSTITUTE OF TECHNOLOGY, CUDDALORE, TAMILNADU

* Corresponding author: paulsam74@gmail.com

TABLE 1

Chemical composition of Udimet L-605 alloy

Cobalt, Co	Chromium, Cr	Tungsten, W	Nickel, Ni	Iron, Fe	Others
46.38-56.5%	19-21%	14-16%	9-11%	≤3%	Remainder

many studies had done before. The table revealed that it was mostly made of alloys with high chromium content. The turning procedure generally appears to be very difficult, notwithstanding the literature study's preference for titanium alumina nitride coated with a titanium nitride cutting insert.

3. Experimental setup

Experiments are carried out on all geared lathe the experiments are designed by using design of experiments. The L9 orthogonal array was used for this investigation. L9 orthogonal approach was mostly used in all of the research studies to predict the optimum parameters. The levels and its stages are clearly mentioned on the TABLE 2.

TABLE 2

Machining variables for turning test

Parameters	Level 1	Level 2	Level 3
Cutting speed (m/min)	40	60	80
Feed rate (mm/rev)	0.04	0.06	0.08
Depth of cut mm	0.5	0.75	1.00

Fig. 1 gave a good illustration of the experiment's technique. The L9 orthogonal array was used for conduct the nine experiments. As the work piece, fresh, readily available udimet alloy was used. Investigating tool wear and the surface morphology of the machined surface is the goal of this investigation. Cut depth, feed rate, and cutting speed were the input limitations. Surface roughness and tool tip temperature are the output or response variables. An infrared thermometer was installed on the tool post of the lathe and its focus point was set to the cutting zone. Three locations around the perimeter of the work piece were used to compute the tooltip temperature for each run, and

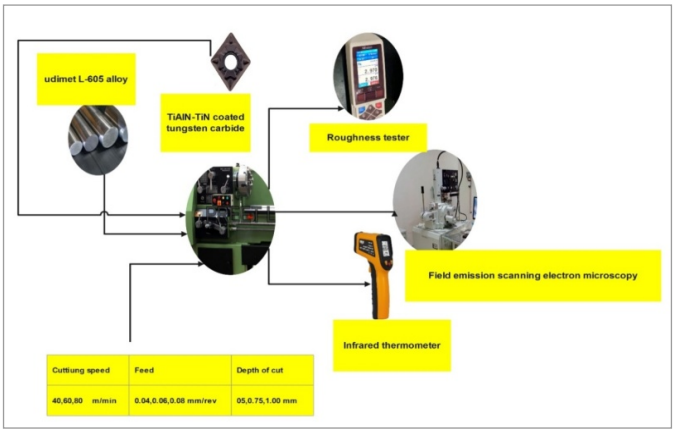

Fig. 1. Experimental methodologies

the average value was obtained and recorded in the output data. The work piece was fixed on a v-block at the conclusion of each experiment, and using a surface roughness tester, the roughness values were measured at three different spots on the surface, with the average value being taken into consideration. Following the measurement, the tool wear was precisely tracked using the tool maker's microscope, and two tool inserts were selected as a sample. Depending on how worn out the tool was, it was placed in the high- and low-damaged tool categories. The wear patterns could be seen clearly in the SEM images that were captured using a field-effect scanning electron microscope. Additionally, the machined surface's high and low surface finishes must be considered. An atomic force microscope was used to study the surface morphology. The values are recommended from the literature study.

TABLE 3

Output results

Input variables				Output variables	
Runs	Speed (m/min)	Feed (mm/rev)	Depth of cut (mm)	Durface roughness (microns)	Tool tip temperature (deg C)
1	40	0.04	0.5	1.28	225
2	40	0.06	0.75	2	240
3	40	0.08	1	2.92	270
4	60	0.04	0.75	1.92	251
5	60	0.06	1	2.84	262
6	60	0.08	0.5	1.51	238
7	80	0.04	1	3	280
8	80	0.06	0.5	1.21	218
9	80	0.08	0.75	2.8	255

It was confirmed by TABLE 3 that as feed rate and depth of cut increased, so did surface roughness and tool tip temperature. The hardest material used in machining causes the greatest forces to be directed at the cutting tool during the machining process. The temperature of the tool tip increased as a result of the sharp increase in the rubbing action between the cutting tool and the work piece. The chattering motion between the tool and work piece is automatically produced when the force is significantly raised during the turning process. As was also plainly shown in the output data, it has an impact on the surface finish. Fig. 2 clearly showed the primary effect plot for the goal function. The major goal of this study is to reduce the output constraints by optimizing the input variables. Each factor's contribution to reducing the output parameters is shown in Fig. 2. According to the figure, output variables such tool tip temperature, surface roughness, and tool wear are minimized when the minimum speed, moderate feed rate, and reduced cutting depth are used. Depth of cut has the most contribution to accomplishing the target

function; this is demonstrated by level 1 estimated in the response table connected to the image. Feed rate is the second crucial element, which was also seen in Fig. 2.

PVD coated tool has more reliability and more wear resistance compared with CVD coated tool. For better thermal stability, low coefficient of friction, excellent wear resistance, longer tool life and high heat carrying capacity the above tool was used.

4. Results and discussion

4.1. Cutting temperature

Due to the cutting tool's tribological performance, the rubbing action between the tool and work piece produces increased friction and a high temperature in the cutting zone. The high strength of the super alloy Udimet L-605 in this study resulted in a significant rise in the cutting zone temperature. The cutting wears out quickly and has an impact on the work material's surface finish because of the characteristics of the work material. At its highest temperature, udimet alloy produces increased yield strength, which has an impact on the turning tool's performance. The udimet alloy L-605's thermal conductivity was discovered to be 9.40 W/mk, which seems incredibly low when compared to other steel compositions. Thermal conductivity is low according to this attribute. This characteristic causes tools to absorb more heat and wear out more quickly than when working with other steels. At a speed of 80 m/min, a feed rate of 0.04 mm/rev, and a cutting depth of 1 mm, a temperature in the cutting zone of roughly 2800 C was discovered. The eighth run had the lowest temperature recorded; it was attained with the shallowest cut, and a modest feed rate was noted. The infrared thermometer used in this study has temperature range – 50°C-330°C, response time – 500 ms and accuracy ±0.10°C. During the machining process the tool tip temperature was measured at three intervals and the average value was taken.

4.2. Surface roughness

In general, it was discovered that as the frictional force between the tool and the work piece grew, the surface roughness value gradually rose. The most important factors in increasing and decreasing the surface roughness value of the machined object are feed rate and depth of cut. The surface roughness value was found to be at its peak at the seventh run, as can be seen from the graphical representation in Fig. 2. On the second and fifth runs, it was likewise keeping the widest possible range. According to TABLE 3's observations, as the depth of cut automatically increases, the surface roughness value sharply rises and results in a poor surface finish on the machined part. The eighth run yielded the lowest surface roughness rating, which was mostly a result of the machining operation's decreased depth of cut and moderate feed rate.

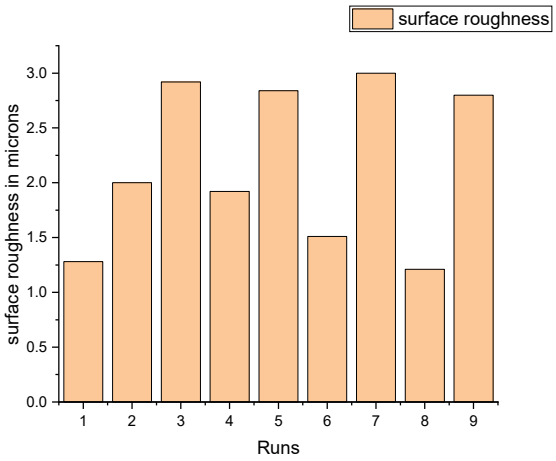

Fig. 2. Graphical plot of surface roughness

4.3. Tool wear

After the machining, a SEM test was performed on each cutting tool insert to confirm that the failure mode occurred on the surface. The distinct tool wear patterns in each of the nine cutting tool insert SEM pictures were clearly examined. Edge chipping, which was present on the cutting tool, was the most typical type of tool wear. In this investigation, Fig. 3a) shows that the tool SEM image was captured while being machined at a moderate feed rate, maximum depth of cut, and cutting speed. Fig. 3b) shows the cutting tool's SEM picture under the machining conditions of a shallow cut and a steady feed rate. Due to the greater cutting zone temperature of 2800C created at the cutting zone due to the high depth of cut (see Fig. 3a), it was badly impacted by flank wear. In addition to the deeper the cut, the lesser thermal conductivity of the work material also contributes to increased flank wear. The cutting tool insert absorbs all the heat, rupturing as a result. A built-up edge was also observed in a few spots; this was caused by strong frictional forces; the coating of the cutting tool insert delaminated, and the work piece's weldment was deposited on the tool. The most frequent issue was edge chipping because of the maximum depth of cut. Due to

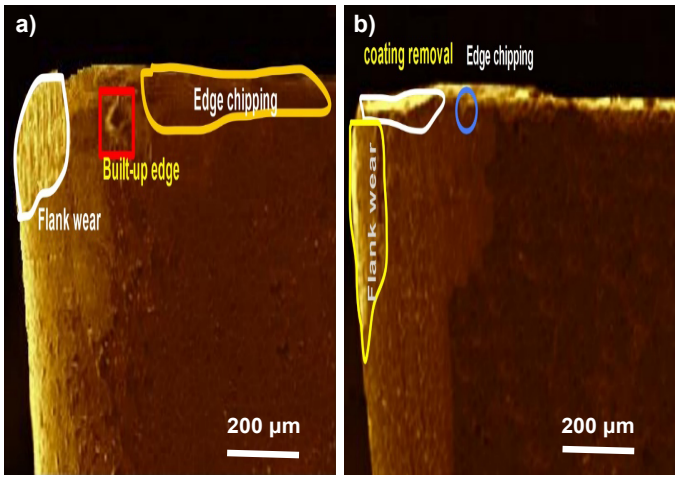

Fig. 3. SEM images of the cutting tool after machining a) 7th run b) 8th run

the characteristics of the work piece and the cutting tool, slight flank wear was formed in some areas of Fig. 4b. Due to abrasive action occurring between the tool and work piece, coating loss was also seen on the top surface. The tool edge also showed the least degree of edge chipping, which was readily apparent. It indicates the wear pattern like crater, bulk formation, chip adhesion, pitting of work material after machining.

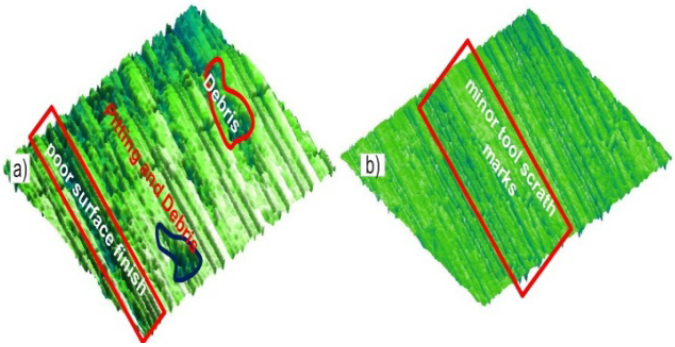

Fig. 4. surface morphology of the machined surface a)7th run b) 8th run

4.4. Surface morphology

The image of the machined surface captured by an atomic force microscope is shown in Fig. 4. It was imperative to look into how the surface topography altered in relation to the output variables, such as tool tip temperature and surface roughness, when the associated input parameters were modified. The machined piece was 100 microns by 100 microns in size for the AFM research. With the help of the wireelectric discharge machining method, it was removed from the surface of the work piece. After the AFM was acquired, it was processed and nicely displayed in Fig. 4. The AFM of the workpiece surface that was machined with a deeper cut and a faster feed rate is shown in Fig. 4(a). A poor surface finish occurs from the blunt edge that is created on the cutting tool as a result of increased cutting (or abrasive) action between the tool and workpiece. This increased frictional force also results in increased thermal load on the tool. Additionally, it causes the workpiece to develop pits, and in some spots, debris was also produced as a result of chips being welded to the workpiece. Fig. 4(b) shows a workpiece surface where there is no pitting and no debris accumulation as a result of the minimal cutting depth and moderate feed rate. Only low-level tool scratches were seen.

These are the two important parameters which is used to identify the surface profile and characterization after the machining.

The surface profile of the machined surface for the seventh and eighth runs, respectively, is shown in Figs. 5 and 6. An AFM study was conducted to examine the surface topography in depth. AFM study is used to see the peak and valley profiles generated on the surface for simple identification of wear and fault patterns on the machined surface. It is the best method for representing the 3D image of the profile. The roughness, waviness, and texture profile of the machined surface were investigated by a study on surface characterization. The roughness average, root mean square, average maximum height of the roughness, valley depth, kurtosis, and skewness were the surface parameters for this investigation. The values were precisely determined, and TABLE 4 clearly summarized them. The machined surface's average roughness value was noted on the seventh run due to a subpar surface finish. The value was nearly 93.38 nm, or roughly three times the surface that was cut on the eighth run. It means that on the eighth run, the surface finish on the machined surface was only good. The surface machined at a higher depth of cut and feed rate had a greater maximum height of roughness and valley depth due to the workpiece being cratered and pitted by excessive heat and frictional forces. The seventh specimen's skewness value, which was determined to be 0.1191, corresponds to a few surface-created spikey profiles. Additionally, it is discovered that the kurtosis value is 3.526, indicating that the profile contains several peak points caused by tool abrasion and pitting markings. The profile was incredibly flat, as evidenced by the fact that it was 6.536 on the eighth specimen at the same time.

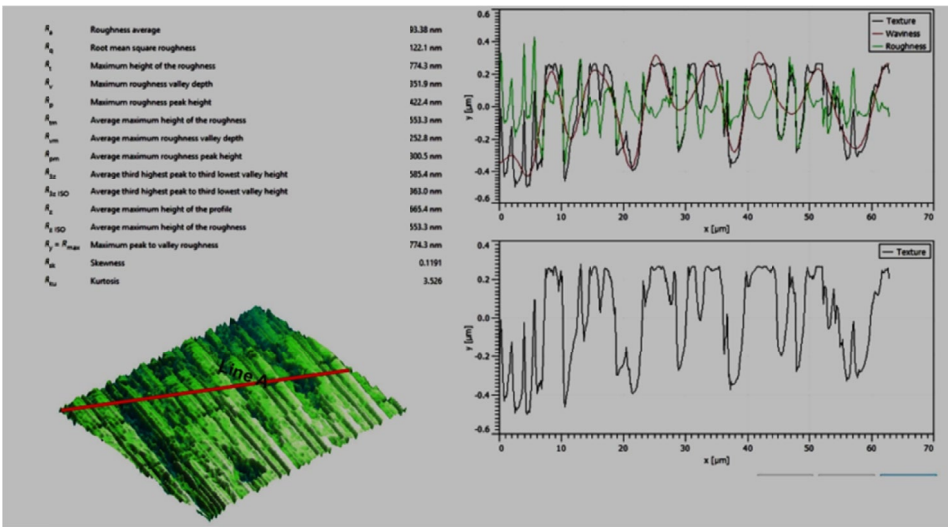

Fig. 5. Surface characterization of the machined surface for the 7th run

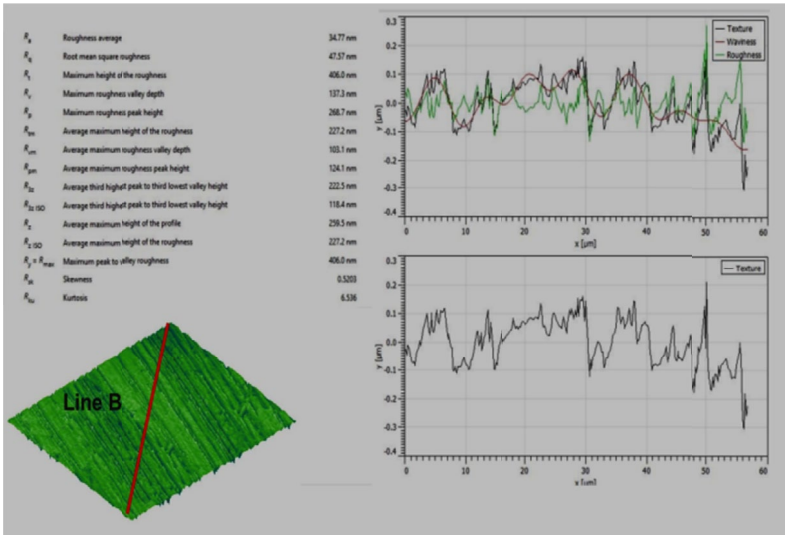

Fig. 6. Surface characterization of the machined surface for the 8th run

TABLE 4

Surface parameters

S.No	Surface parameters	Machined surface for the 7th run	Machined surface for the 8th run
1	Roughness average	93.38 nm	34.77 nm
2	Root mean square	122.1 nm	47.57 nm
3	Average maximum height of the roughness	553.3 nm	227
4	Valley depth	351.9 nm	137.3 nm
5	skewness	0.1191	0.52
6	kurtosis	3.526	6.536

Particle size analysis

Fig. 7 depicts the SEM picture of the Udimet alloy's machined surface after trials 7 and 8, respectively. According to the figure, it has a higher number of abrasion marks, debris crater development, and binding up with coated particles from the cutting tool during the machining process. The AFM pictures presented in Fig. 4 also corroborated this. The purpose of this research is also to investigate the effect of coated particles on the machining of udimet alloy. Evaluation of the size of the particles that had clustered and separated from the work piece was one of the objectives of this investigation. The first step in calculating particle size is to convert the SEM image into a threshold image. The threshold image is created by converting the gray picture of the SEM image into a binary image that is solely black and white. The threshold picture is used to highlight the particles on the machined surface. Fig. 8 clearly demonstrates this. It was refined in Fig. 9 by numbering the particles embedded on the machined surface. Fig. 9a depicts particles surrounded by numbers smaller than those in Fig. 9 b. It was confirmed that the machined surface in the eighth experiment has greater wear, temperature, and poor surface finish due to particle ploughing during machining. Additionally, supporting evidence came from findings that the tool tip temperature and surface roughness were higher than expected.

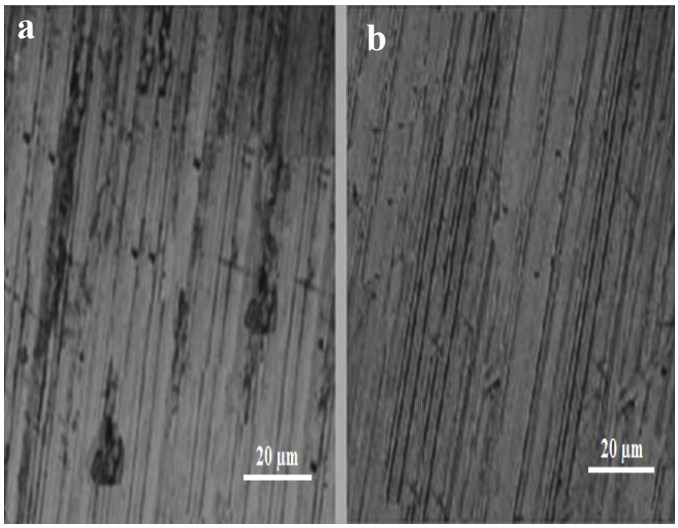

Fig. 7. SEM image of the machined surface of udimet-705 alloy machined at a) 7th run b) 8th run

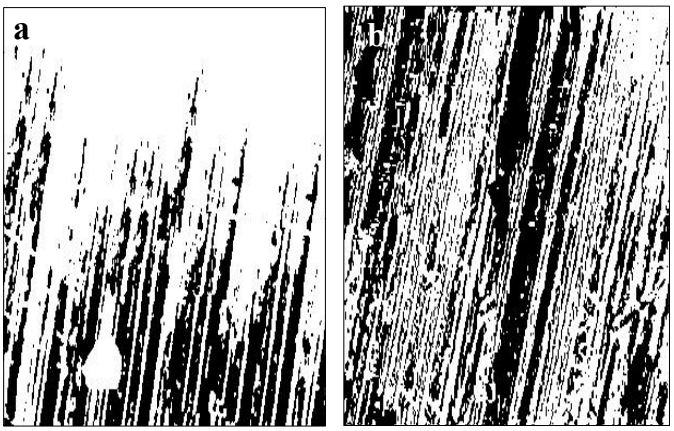

Fig. 8. Threshold image of the machined surface of the udimet-705 alloy specimen at 7th run b) 8th run

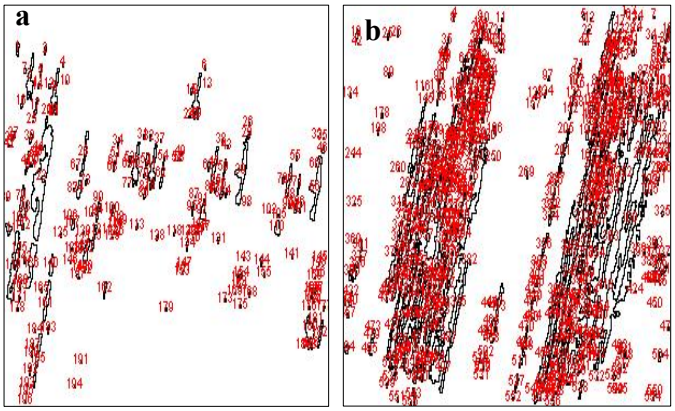

Fig. 9. Particle size identification of the machined surface at a) 7th run b) 8th run

Figs. 10 and 11 illustrate the particle size area distribution of the udimet alloy machine's machined surface at the 7th and 8th runs, respectively. According to Fig. 10, the maximum particle size area is 65 square microns. It refers to workpiece pitting and debris. The average particle area was determined from the graph at approximately 26 square microns. According to Fig. 11, the highest particle size area was discovered to be 55 square microns, and due to increased abrasion marks caused by tool action, particles with an average size area of 15 square microns are deposited on the surface.

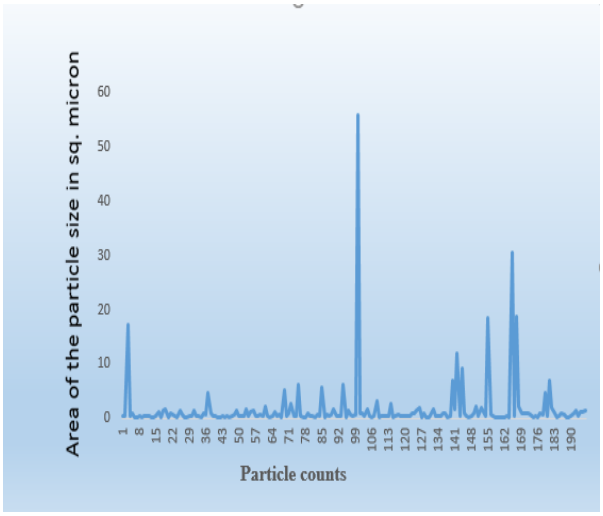

Fig. 10. Particle size distribution of the machined surface at 7th run

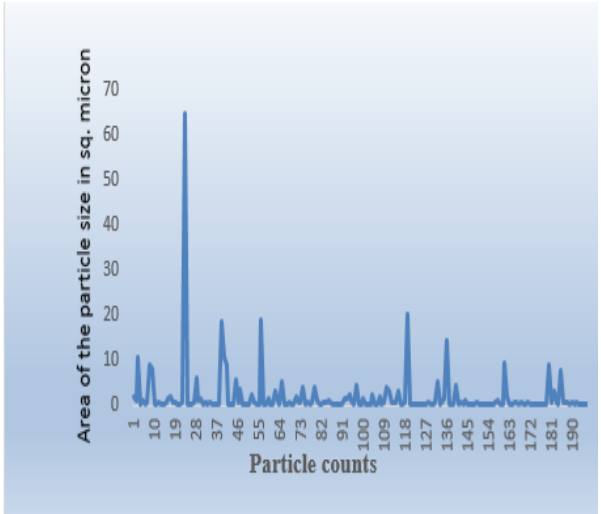

Fig. 11. Particle size distribution of the machined surface at 8th run

5. Conclusion

In the past research study a few researchers are concentrated on the super alloy udimet L-605 alloy and they are more concentrated on the unconventional machining process.

- In this study the machining parameters were successfully investigated at different cutting speed, feed rate and depth of cut.
- Depth of cut was considered as the most contributing factors to minimize the output variables such as tool tip temperature and surface roughness, nearly 100% increase in the surface roughness when the depth increases from lowest variable to highest variable as 1 mm. nearly 23% tool tip interface temperature was increases with increase in depth of cut.
- The average roughness of 34.77 nm was attained.
- Surface morphology was carried out on the machined surface and discuss about the surface parameters and its effect on surface roughness and surface behavior on the work material.
- Particle size analysis was carried on the machining surface. The average particle area was determined from the graph at approximately 26 square microns.

REFERENCES

[1] Y.S. Kong, M. Cheepu, D.G. Kim, Effects of Heat Treatment on the Mechanical Behavior of Udimet 720 Nickel-Based Superalloy. J. Mater. Eng. Perform **31**, 8327-8333 (2022). DOI: https://doi.org/10.1007/s11665-022-06858-6

[2] Y.S. Kong, J. Yu, Y.W. Park, Creep Life Prediction of Alloy 718 for Automotive Engine Materials. Int. J. Automot. Technol. **19** (6) 1055-1059 (2019).

[3] R. Jerez-Mesa, V. Plana-García, J. Llumà, J.A. Travieso-Rodriguez, Enhancing surface topology of Udimet 720 super alloy through ultrasonic vibration-assisted ball burnishing. Metals **10** (7) 915-920 (2020).

[4] S. Dubiez-Le Goff, R. Couturier, L. Guétaz, H. Burlet, Effect of the microstructure on the creep behavior of PM Udimet 720 superalloy – experiments and modeling. Materials Science and Engineering A **387**, 599-603 (2005).

[5] S. Behera, M.K. Dash, N.K. Kumar, R. Mitra, G.A. Rao, Microstructure and High-Temperature Tensile Behavior of Ni-Based Superalloy EP741NP for Aerospace Applications. J. Mater. Eng. Perform. **30** (8) 5834-5844 (2021).

[6] N.A. Özbek, M.I. Karadag, O. Özbek, Optimization of flank wear and surface roughness during turning of AISI 304 stainless

steel using the Taguchi method. Materials Testing **62** (9) 957-961 (2020).

[7] E. Nas, N. AltanÖzbek, Optimization of the machining parameters in turning of hardened hot work tool steel using cryogenically treated tools. World Scientific Connect **27** (5), 1-10 (2020). DOI: https://doi.org/10.1142/S0218625X19501774

[8] G. Basmaci, A.S. Yoruk, U. Koklu, S. Morkavuk, Impact of cryogenic condition and drill diameter on drilling performance of CFRP. Appl. Sci. **7** (7), 667-675 (2020).

[9] D. Fernández, A. Sandá, I. Bengoetxea, Cryogenic milling: Study of the effect of CO_2 cooling on tool wear when machining Inconel 718, Grade EA1N Steel and Gamma TiAl. Lubricants **7** (1), 10-17 (2020).

[10] L. Proud, N. Tapoglou, T. Slatter, A review of CO2 coolants for sustainable machining. Metals **12** (2) 283-290 (2022).

[11] O. Özbek, H. Saruhan, The effect of vibration and cutting zone temperature on surface roughness and tool wear in eco-friendly MQL turning of AISI D2. J. Mater. Res. Technol. **9** (3), 2762-2772 (2022).

[12] V. Baldin, L. Rosa Ribeiro da Silva, C.F. Houck, R.V. Gelamo, A.R. Machado, Effect of Graphene Addition in Cutting Fluids Applied by MQL in End Milling of AISI 1045 Steel. Lubricants **9**, 70-80 (2021).

[13] A.M. Khan, M. Jamil, M. Mia, D.Y. Pimenov, V.R. Gasiyarov, M.K. Gupta, N. He, Multi-objective optimization for grinding of AISI D2 steel with Al2O3 wheel under MQL. Materials **11** (11) 2269-2278 (2018).

[14] O.A. Bég, D.S. Espinoza, A. Kadir, M.D. Shamshuddin, A. Sohail, Experimental study of improved rheology and lubricity of drilling fluids enhanced with nano-particles. Appl. Nanosci. **8**, 1069-1090 (2018).